Seismic wave attenuation and dispersion due to wave-induced fluid flow in rocks with strong permeability fluctuations

J. Germán Rubino[a)]
Applied and Environmental Geophysics Group, University of Lausanne, Lausanne, Switzerland

Leonardo B. Monachesi
CONICET, Facultad de Ciencias Astronómicas y Geofísicas, Universidad Nacional de La Plata, La Plata, Argentina

Tobias M. Müller
Earth Science and Resource Engineering Division, Commonwealth Scientific and Industrial Research Organization, Perth, Australia

Luis Guarracino
CONICET, Facultad de Ciencias Astronómicas y Geofísicas, Universidad Nacional de La Plata, La Plata, Argentina

Klaus Holliger
Applied and Environmental Geophysics Group, University of Lausanne, Lausanne, Switzerland

Oscillatory fluid movements in heterogeneous porous rocks induced by seismic waves cause dissipation of wave field energy. The resulting seismic signature depends not only on the rock compressibility distribution, but also on a statistically averaged permeability. This so-called equivalent seismic permeability does not, however, coincide with the respective equivalent flow permeability. While this issue has been analyzed for one-dimensional (1D) media, the corresponding two-dimensional (2D) and three-dimensional (3D) cases remain unexplored. In this work, this topic is analyzed for 2D random medium realizations having strong permeability fluctuations. With this objective, oscillatory compressibility simulations based on the quasi-static poroelasticity equations are performed. Numerical analysis shows that strong permeability fluctuations diminish the magnitude of attenuation and velocity dispersion due to fluid flow, while the frequency range where these effects are significant gets broader. By comparing the acoustic responses obtained using different permeability averages, it is also shown that at very low frequencies the equivalent seismic permeability is similar to the equivalent flow permeability, while for very high frequencies this parameter approaches the arithmetic average of the permeability field. These seemingly generic findings have potentially important implications with regard to the estimation of equivalent flow permeability from seismic data. © 2013 Acoustical Society of America. [http://dx.doi.org/10.1121/1.4824967]

I. INTRODUCTION

Seismic waves propagating in fluid-saturated porous rocks with heterogeneity in the mesoscopic scale range, that is, heterogeneities larger than the pore size but smaller than the prevailing wavelengths, can be significantly attenuated (e.g., Pride *et al.*, 2004; Müller *et al.*, 2010). This is because seismic waves induce a local, oscillatory fluid flow between mesoscale heterogeneities with differing elastic compliances. This so-called wave-induced fluid flow (WIFF) loss mechanism depends on the rock properties as well as on the pore fluid composition. Specifically, WIFF depends on the hydraulic transport capability of the rock, that is, the flow permeability. This dependence can be readily understood as WIFF implies fluid pressure diffusion between different mesoscale heterogeneities of the probed rock volume. The fluid pressure diffusivity, in turn, is directly proportional to

the flow permeability. Therefore, the WIFF mechanism provides a link between flow permeability and seismic attributes. Implications of this link have been exemplified in some contexts (e.g., Rubino *et al.*, 2012). Flow permeability estimates extracted from seismic signals would have enormous value for underground reservoir characterization, with potential applications in hydrocarbon exploration, hydrology, and geotechnical engineering (e.g., van Dalen *et al.*, 2010).

Flow permeability is arguably one of the most variable parameters in geological formations, including sedimentary basins and aquifers. Even in seemingly homogeneous formations it may range over several orders of magnitude (e.g., Sanchez-Vila *et al.*, 2006). Thus, from a seismic point of view it seems expedient to search for an *equivalent seismic permeability*. This permeability is defined such that it results in the same amount of attenuation and phase velocity dispersion due to WIFF when the actual heterogeneous permeability field is upscaled and replaced by a constant value. In this context, it is, however, important to note that the equivalent seismic permeability is different from the

[a)]Author to whom correspondence should be addressed. Electronic mail: german.rubino@unil.ch

dynamic permeability used to model the transition from the viscosity- to the inertia-dominated flow regime in Biot's (1956a,b) theory (e.g., Johnson *et al.*, 1987; Müller and Sahay, 2011).

Shapiro and Müller (1999) showed that in randomly layered poroelastic media there is a discrepancy between the equivalent seismic permeability and the *equivalent flow permeability,* that is, the permeability obtained by upscaling the flow equations. More recently, Müller *et al.* (2007) showed that in weakly heterogeneous random poroelastic media the equivalent seismic permeability is frequency-dependent. Only in the low-frequency limit does the equivalent seismic permeability coincide with the flow permeability. This means that the equivalent seismic permeability should actually be a dynamic-equivalent permeability.

In order to understand the role of permeability fluctuations for the WIFF loss mechanism, the following analytical recipe has been developed. Based on the method of statistical smoothing applied to Biot's (1956a) equations, Müller *et al.* (2007) derived a dispersion equation for the slow compressional wave in the presence of permeability fluctuations. From this dispersion equation, an equivalent seismic permeability can be identified that shows dynamic behavior in the seismic frequency band. This dynamic-equivalent permeability model can then be incorporated into the expression for the dynamic-equivalent wavenumber for the fast compressional wave also obtained by the method of statistical smoothing. This wavenumber entails attenuation and velocity dispersion due to WIFF taking into account random permeability fluctuations. It has been inferred that permeability fluctuations cause WIFF to be observable in a broader frequency range and that the peak attenuation shifts along the frequency axis depending on the strength of the permeability fluctuations. Müller *et al.* (2007) extended this analysis to strong permeability fluctuations in randomly layered media and observed good agreement with the attenuation and velocity dispersion obtained from numerical simulations.

The above recipe does, however, have several limitations mainly associated with the difficulty of treating strong fluctuations by means of perturbation theory methods. Therefore, it is not known how strong permeability fluctuations affect seismic signatures due to WIFF. This problem is not only of obvious interest in the context of flow permeability extraction from seismic signatures, but also presents a challenge from a theoretical point of view. For 1D random media, the exact low- and high-frequency limits of the equivalent seismic permeability are known and application of the strong-contrast perturbation theory reveals the frequency-dependence of this dynamic-equivalent permeability (Caspari *et al.*, 2013). However, the corresponding results for 2D or 3D random media have not been obtained, which is also due to the fact that there are no analytical solutions for the effective flow permeability (e.g., Sanchez-Vila *et al.*, 2006).

The aim of this work is to quantify the impact of strong permeability fluctuations on the WIFF mechanism. This is done through numerical simulations in 2D realizations of random fields including strong permeability fluctuations. The random medium parameters are chosen such that they mimic typical porous rocks. To determine seismic attenuation and velocity dispersion due to WIFF, we use a numerical oscillatory compressibility test based on the quasi-static poroelasticity equations, similar to that proposed by Rubino *et al.* (2009). We compare the simulated attenuation and velocity dispersion characteristics with those obtained by replacing the fluctuating permeability field by its respective arithmetic and harmonic average, as well as by the true equivalent flow permeability. The latter is numerically inferred from a separate upscaling procedure based on the steady-state flow equations. These broadband simulations provide further insight into the role of the equivalent seismic permeability for attenuation and velocity dispersion. Similar questions to those addressed here at the mesoscopic scale have previously been analyzed in the framework of Biot's (1956a,b) intrinsic attenuation mechanism. In this sense, Berryman (1986, 1988) determined the correct permeability average in the context of this attenuation mechanism, while Yamamoto and Turgut (1988) analyzed the effects of the pore size distribution on the frequency dependence of this energy loss mechanism.

This paper is organized as follows. First, we introduce the numerical methodologies of the quasi-static oscillatory compressibility and steady-state flow tests. While the former test allows us to infer compressional wave attenuation and velocity as functions of frequency, the latter test yields the true equivalent flow permeability. This is followed by a series of numerical simulations involving 2D binary random medium realizations. Changes in the attenuation and dispersion behaviors caused by the associated permeability fluctuations are analyzed and discussed.

II. METHODOLOGICAL BACKGROUND

A. Spatial and temporal scales of WIFF

WIFF constitutes an important attenuation mechanism in porous rocks, which is operative in the presence of heterogeneities in the mesoscopic scale range. This means that the characteristic length scale of the heterogeneities a_{meso} satisfies the relation

$$a_{\mathrm{pore}} \ll a_{\mathrm{meso}} \ll \lambda, \tag{1}$$

where a_{pore} represents a typical pore or grain size and λ is the predominant seismic wavelength. The propagation of seismic waves through a medium containing mesoscopic heterogeneities produces local fluid pressure gradients and fluid flow. The associated fluid pressure relaxation is therefore governed by fluid pressure diffusion with a characteristic transition frequency, ω_c. This characteristic frequency depends on the size of the mesoscopic heterogeneities and the scales at which fluid flow occurs, that is, the corresponding diffusion lengths involved in the process. At this characteristic frequency, the diffusion length, L_d, is of similar size as the heterogeneities, so that

$$L_d \equiv \sqrt{D/\omega_c} \simeq a_{\mathrm{meso}}, \tag{2}$$

or equivalently,

J. Acoust. Soc. Am., Vol. 134, No. 6, Pt. 2, December 2013

Rubino *et al.*: Dynamic permeability of rocks   4743

$$\omega_c \simeq D/a_{\text{meso}}^2, \tag{3}$$

where D is the pressure diffusivity. This parameter can be expressed in terms of the poroelastic properties of the fluid-saturated porous rock (e.g., Rubino *et al.*, 2012)

$$D = \frac{\kappa}{\eta} \left(\frac{LM - \alpha^2 M^2}{L} \right), \tag{4}$$

where κ and η denote the permeability of the rock and the fluid shear viscosity, respectively. In addition, the parameters α, M, and L are given by (e.g., Rubino *et al.*, 2012)

$$\alpha = 1 - \frac{K_m}{K_s}, \tag{5}$$

$$M = \left(\frac{\alpha - \phi}{K_s} + \frac{\phi}{K_f} \right)^{-1}, \tag{6}$$

$$L = \lambda_u + 2\mu. \tag{7}$$

In these expressions, K_s, K_m, and K_f are the bulk moduli of the solid grains, the dry matrix and the fluid phase, respectively, while μ is the shear modulus of the bulk material, which is equal to that of the dry frame, and ϕ is the porosity of the rock. In addition, the saturated Lamé parameter, λ_u, is given by

$$\lambda_u = K_{\text{sat}} - \frac{2}{3}\mu, \tag{8}$$

where K_{sat} is the undrained bulk modulus of the saturated material, which can be computed as (e.g., Rubino *et al.*, 2012)

$$K_{\text{sat}} = K_m + \alpha^2 M. \tag{9}$$

For frequencies $\omega \ll \omega_c$, the diffusion lengths are much larger than the typical size of the heterogeneities. Correspondingly, there will be enough time during each oscillatory half cycle for the fluid pressure to equilibrate at a common value. Thus, this low-frequency regime represents a relaxed state. On the other hand, for frequencies $\omega \gg \omega_c$. the diffusion lengths are very small compared to the size of the heterogeneities. There is no time for communication between the pore fluid of the different parts of the rock. In this case, the pore pressure is approximately constant within each heterogeneity and, consequently, this high-frequency regime is associated with an unrelaxed state. For intermediate frequencies, as characterized by diffusion lengths that are of similar size as the heterogeneities, that is, frequencies ω close to ω_c, significant fluid flow can be induced by the seismic wave, which in turn can generate significant attenuation and velocity dispersion effects. Thus, the characteristic frequency ω_c defined by Eq. (3) is also associated with maximum attenuation due to WIFF. From Eqs. (3) and (4), we notice that the frequency range where attenuation due to WIFF operates shifts toward lower frequencies for decreasing permeability and increasing fluid viscosity or size of the mesoscopic heterogeneities.

The propagation of seismic waves in porous elastic solids saturated by compressible viscous fluids can be modeled using the theory of poroelasticity developed by Biot (1956a,b). Biot considered a porous isotropic medium saturated with a single-phase, compressible viscous fluid. He further assumed that anelastic effects arise from relative motions between the fluid and the solid frame. One of the most important consequences of Biot's work is the prediction of a slow compressional wave, in addition to the classical compressional (P) and shear (S) waves known in classical elastodynamics. This additional wave, commonly referred to as P_2 or slow Biot wave, is characterized by a phase velocity lower than that of the P wave and is associated with an out-of-phase motion of the solid and fluid phases. An important parameter in this theory is the critical Biot frequency ω_{Biot} (Biot, 1956a,b). This critical frequency separates the viscosity-dominated regime ($\omega \ll \omega_{\text{Biot}}$) from the regime dominated by the inertial forces ($\omega \gg \omega_{\text{Biot}}$). In the viscosity-dominated or low-frequency range, the P_2 wave is strongly attenuated and, actually, is not a propagating mode but a fluid pressure diffusion process (Dutta and Odé, 1979; Chandler and Johnson, 1981). In the high-frequency range, the P_2 mode is a propagating wave. In the framework of the Biot (1956a) theory, seismic attenuation due to WIFF can be seen as energy conversion from the classical wave propagating through the heterogeneous domain into P_2-wave energy at the discontinuities of the rock (Gurevich and Lopatnikov, 1995; Müller and Gurevich, 2005a,b). Because of their diffusive nature, these P_2 waves cannot directly be observed in the low-frequency range. However, we can infer their existence as they may be responsible for the observed attenuation levels of the propagating waves modes due to WIFF effects.

B. Quasi-static poroelasticity and the oscillatory compressibility test

Studying seismic attenuation and velocity dispersion due to WIFF at mesoscopic scales is a difficult task. This is mainly due to the fact that, in the low-frequency range, the diffusion process associated with the fluid pressure equilibration is a critical issue because the corresponding diffusion lengths, which characterize the spatial scales at which the fluid pressure equilibration or fluid flow occurs, are very small as compared with the seismic wavelengths (e.g., Rubino *et al.*, 2007). This, in addition to the necessity to consider small enough grid spacing to properly represent the mesoscopic heterogeneities, is an issue both in the low- and high-frequency ranges.

Rubino *et al.* (2009) proposed an upscaling procedure based on a numerical oscillatory compressibility test for representative rock samples having an isotropic distribution of mesoscopic heterogeneities. This methodology permits one to obtain the equivalent complex undrained plane wave moduli, which contain the information on attenuation and velocity dispersion due to WIFF. We use this methodology to solve Biot's (1941) consolidation equations rather than Biot's (1956a) equations of motion, as it has also been suggested by Wenzlau *et al.* (2010) and Quintal *et al.* (2011).

4744   J. Acoust. Soc. Am., Vol. 134, No. 6, Pt. 2, December 2013

Rubino *et al.*: Dynamic permeability of rocks

That is, since WIFF is controlled by fluid pressure diffusion, we can neglect the inertial forces that, in turn, provide us a more efficient procedure to estimate WIFF effects. To this end, we solve the equations of quasi-static poroelasticity in the space-frequency domain (Biot, 1941)

$$\nabla \cdot \boldsymbol{\sigma} = \mathbf{0}, \tag{10}$$

$$i\omega \frac{\eta}{\kappa} \boldsymbol{w} = -\nabla p_f, \tag{11}$$

where $\boldsymbol{\sigma} \equiv (\sigma_{ij})$ is the stress tensor, $\boldsymbol{w}$ is the relative fluid–solid displacement, and p_f is the fluid pressure. Please note that Eq. (10) represents the stress equilibrium within the sample, whereas the expression (11) is Darcy's law. These two equations are coupled through the stress-strain relations

$$\sigma_{ij} = 2\mu\epsilon_{ij}(\boldsymbol{u}^s) + \delta_{ij}(\lambda_u \nabla \cdot \boldsymbol{u}^s - \alpha M\zeta), \tag{12}$$

$$p_f = -\alpha M \nabla \cdot \boldsymbol{u}^s + M\zeta, \tag{13}$$

where $\boldsymbol{u}^s$ denotes the average displacement vector of the solid phase, $\epsilon_{ij}(\boldsymbol{u}^s) = \frac{1}{2}(\partial u_i^s/\partial x_j + \partial u_j^s/\partial x_i)$ is the strain tensor of the solid phase and $\zeta = -\nabla \cdot \boldsymbol{w}$ represents the change in fluid content.

To compute WIFF effects, we consider representative rock samples in the form of rectangular random medium realizations containing mesoscopic-scale heterogeneities. These media are subjected to a time-harmonic compression with constant amplitude of the form $\Delta Pe^{i\omega t}$ on its upper boundary, and no tangential forces act on the boundaries. The solid phase is neither allowed to move on the lower boundary nor have horizontal displacements on the lateral boundaries. Further, the fluid is not allowed to flow into or out of the numerical domain.

Denoting by V the original volume of the sample, its complex oscillatory volume change $\Delta V(\omega)$ allows us to define the *equivalent* undrained complex plane-wave modulus, $\bar{L}(\omega)$, by using the relation

$$\frac{\Delta V(\omega)}{V} = -\frac{\Delta P}{\bar{L}(\omega)}, \tag{14}$$

which is valid for a viscoelastic homogeneous solid in the quasi-static case. In order to estimate this volume change, Eqs. (10) to (13) are solved under proper boundary conditions. Let $\Omega = (0, L_x) \times (0, L_y)$ be a domain in the (x,y)-plane representing the rock sample to be compressed. Set Γ the boundary of Ω, given by $\Gamma = \Gamma^L \cup \Gamma^B \cup \Gamma^R \cup \Gamma^T$, where

$$\Gamma^L = \{(x,y) \in \Gamma : x = 0\}, \tag{15}$$

$$\Gamma^R = \{(x,y) \in \Gamma : x = L_x\}, \tag{16}$$

$$\Gamma^B = \{(x,y) \in \Gamma : y = 0\}, \tag{17}$$

$$\Gamma^T = \{(x,y) \in \Gamma : y = L_y\}. \tag{18}$$

Also, denote by $\boldsymbol{v}$ the unit outer normal on Γ and let $\boldsymbol{\chi}$ be a unit tangent so that $\{\boldsymbol{v}, \boldsymbol{\chi}\}$ is an orthonormal system on

Γ. Then, to estimate the volume change $\Delta V(\omega)$, we consider the solution of Eqs. (10) to (13) under the following boundary conditions:

$$\boldsymbol{\sigma v} = (0, -\Delta P), \quad (x,y) \in \Gamma^T, \tag{19}$$

$$\boldsymbol{\sigma v} \cdot \boldsymbol{\chi} = 0, \quad (x,y) \in \Gamma^L \cup \Gamma^R, \tag{20}$$

$$\boldsymbol{u}^s \cdot \boldsymbol{v} = 0, \quad (x,y) \in \Gamma^L \cup \Gamma^R, \tag{21}$$

$$\boldsymbol{u}^s = \mathbf{0}, \quad (x,y) \in \Gamma^B, \tag{22}$$

$$\boldsymbol{w} \cdot \boldsymbol{v} = 0, \quad (x,y) \in \Gamma. \tag{23}$$

The vertical displacements $u_2^s(x, L_y, \omega)$ on Γ^T allow us to obtain an average vertical displacement $u_2^{s,T}(\omega)$ experienced by the boundary Γ^T. Then, for each frequency, ω, the volume change produced by the compressibility test can be approximated by $\Delta V(\omega) \approx L_x u_2^{s,T}(\omega)$, which enables us to compute the equivalent complex plane-wave modulus, $\bar{L}(\omega)$, through Eq. (14). The corresponding complex compressional velocity is given by

$$V_{pc}(\omega) = \sqrt{\frac{\bar{L}(\omega)}{\overline{\rho_b}}}, \tag{24}$$

where $\overline{\rho_b}$ is the average bulk density of the numerical rock sample; that is,

$$\overline{\rho_b} = \frac{1}{V} \int_\Omega (\phi\rho_f + (1-\phi)\rho_s) dV, \tag{25}$$

where ρ_s and ρ_f are the density of solid grains and pore fluid, respectively.

Finally, the equivalent compressional phase velocity, $V_p(\omega)$, and inverse quality factor, $Q_p^{-1}(\omega)$, are then given as (Rubino *et al.*, 2009)

$$V_p(\omega) = \left[\text{Re}\left(\frac{1}{V_{pc}(\omega)}\right)\right]^{-1}, \tag{26}$$

$$\frac{1}{Q_p(\omega)} = \frac{\text{Im}(V_{pc}(\omega)^2)}{\text{Re}(V_{pc}(\omega)^2)}. \tag{27}$$

To estimate the equivalent complex moduli, we employ a finite element procedure to approximate the solution of Eqs. (10) to (13) under the corresponding boundary conditions [Eqs. (19) to (23)]. We use bilinear functions to approximate the solid displacement vector and a closed subspace of the vector part of the Raviart-Thomas-Nedelec space of zero order for the fluid displacement.

It is important to mention that we have performed a 1D convergence analysis to ensure that, given the wide frequency ranges considered in the numerical examples, the employed grid spacing is small enough to properly represent the prevailing fluid pressure diffusion processes.

C. Equivalent flow permeability

In order to infer the discrepancies between the equivalent seismic and flow permeabilities, an additional upscaling procedure to determine the latter is needed. In this sense, the equivalent flow permeability can be obtained using a numerical procedure similar to laboratory tests employed to determine flow permeabilities (Guarracino and Monachesi, 2010). The flow permeability, κ, is defined by the classical Darcy's law through a linear relation between flow velocity, $\dot{w}$, and the gradient of fluid pressure, p_f. Then, the usual procedure to estimate κ experimentally is to prescribe a constant fluid pressure gradient and to measure the fluid discharge through the rock sample.

Fluid flow in saturated porous media is described by the following general equation (Wang, 2000)

$$\frac{\partial \zeta}{\partial t} = -\nabla \cdot \dot{w}. \tag{28}$$

An equivalent value of flow permeability can therefore be obtained by solving Eq. (28) for the steady-state case with boundary conditions that mimic laboratory experiments. Following Desbarats (1992), a predefined fluid pressure difference between the top and bottom boundaries is therefore imposed and no-flow conditions are applied on the lateral boundaries. Then, the corresponding boundary value problem can be expressed as

$$\nabla \cdot \left(\frac{\kappa}{\eta} \nabla p_f \right) = 0, \quad (x, y) \in \Omega, \tag{29}$$

$$p_f = p_1, \quad (x, y) \in \Gamma^B, \tag{30}$$

$$p_f = p_2, \quad (x, y) \in \Gamma^T, \tag{31}$$

$$\dot{w} \cdot \mathbf{v} = 0, \quad (x, y) \in \Gamma^L \cup \Gamma^R, \tag{32}$$

where Eq. (29) is obtained by using Darcy's law (11) in the time domain in Eq. (28) and imposing steady-state conditions.

The numerical solution of the differential problem described by Eqs. (29) to (32) allows us to compute the averaged fluid velocity in the vertical direction, $\overline{\dot{w}}_y$, induced by the externally imposed pressure gradient $\Delta p/L_y = (p_2 - p_1)/L_y$,

$$\overline{\dot{w}}_y = \frac{1}{L_x} \int_{\Gamma^B} \dot{w} \cdot \mathbf{v} \, dx. \tag{33}$$

Then, according to Darcy's law, the equivalent permeability, κ_{eq}, at the scale of the considered rock sample is given by

$$\kappa_{\text{eq}} = \frac{\eta \overline{\dot{w}}_y L_y}{\Delta p}. \tag{34}$$

The differential problem defined by Eqs. (29) to (32) is solved using a mixed finite element method employing the lowest-order Raviart-Thomas-Nedelec space, which gives a simultaneous approximation to fluid pressure and flow. This method is especially suitable for this study because it conserves locally the fluid mass and can handle large

discontinuities in the permeability field (Guarracino and Monachesi, 2010).

III. NUMERICAL ANALYSIS

A. Poroelastic random medium models of heterogeneous porous rocks

In this section, we explore the effects of strong permeability fluctuations associated with spatial porosity variations on the equivalent seismic permeability and its seismic signature. We model a porous rock that is fully saturated with water and whose frame is composed of quartz grains with the poroelastic properties given in Table I. We use the Kozeny-Carman equation to relate porosity, ϕ, of the numerical rock sample to the permeability, κ (e.g., Mavko et al., 2009),

$$\kappa = B \frac{\phi^3}{(1 - \phi)^2} d^2, \tag{35}$$

where B is a geometrical factor that depends on the tortuosity of the sample. In this work, we take $B = 0.003$ and use $d = 8 \times 10^{-3}$ cm for the mean grain diameter.

In addition to permeability fluctuations, a spatially variable porosity also implies fluctuations in other poroelastic parameters, such as the dry frame moduli and bulk density. In fact, considering fluctuations in the elastic properties of the dry frame is essential as poroelastic compressibility contrasts are needed to produce WIFF (e.g., Müller and Gurevich, 2005b). To link the porosity, ϕ, and the solid grain properties with the elastic moduli of the dry frame we use the model of Krief et al. (1990),

$$K_m = K_s (1 - \phi)^{3/(1-\phi)}, \tag{36}$$

$$\mu = K_m \mu_s / K_s, \tag{37}$$

where μ_s is the shear modulus of the solid grains.

We study the behavior of the equivalent seismic permeability in the case of strong permeability fluctuations produced by a heterogeneous binary porosity field. We generate this field using stochastic fractal fields based on a von-Karman-type spectral density function, which is frequently used in the statistical characterization of heterogeneities for different applications (e.g., Tronicke and Holliger, 2005)

TABLE I. Material properties for the models considered in this study.

	Material 1	Material 2
Grain bulk modulus, K_s [GPa]	37	37
Grain shear modulus, μ_s [GPa]	44	44
Grain density, ρ_s [g/cm^3]	2.65	2.65
Porosity, ϕ	0.05	0.4
Dry rock bulk modulus, K_m [GPa]	30	1.25
Dry rock shear modulus, μ [GPa]	35	1.5
Permeability, κ [D]	0.00269	3.458
Water density, ρ_f [g/cm^3]	1.04	
Water bulk modulus, K_f [GPa]	2.25	
Water viscosity, η [Pa $\times$ s]	0.003	

4746   J. Acoust. Soc. Am., Vol. 134, No. 6, Pt. 2, December 2013

Rubino et al.: Dynamic permeability of rocks

$$S_d(k_x, k_y) = S_0(1 + k_x^2 a_x^2 + k_y^2 a_y^2)^{-(H+E/2)}, \qquad (38)$$

where k_x and k_y are the horizontal and vertical wavenumbers, a_x and a_y are the horizontal and vertical correlation lengths, S_0 is a normalization constant, and E is the Euclidean dimension. This expression corresponds to a band-limited scale-invariant stochastic process with a Hausdorff fractal dimension, $D_H = E + 1 - H$, with $0 \leq H \leq 1$.

To generate heterogeneous porosity fields with corresponding characteristics, we first partition the computational domain into a finite number of grid cells Ω_j and assign to each of these cells a pseudo-random number drawn from a uniform distribution. Then, we Fourier transform this field to the spatial wavenumber domain and filter its amplitude spectrum using Eq. (38), with $a_x = a_y = 1$ cm and $H = 1$. Next, we transform back the result to the spatial domain to obtain a heterogeneous field. Finally, the binary field is obtained through thresholding and appropriate rescaling. Please note that this binarization of the original continuous stochastic field results in a halving of the original H-value; that is, $H_{\text{binary}} = H/2 = 0.5$ and $D_H = E + 1 - H_{\text{binary}} = 2.5$ (Holliger *et al.*, 1993; Goff *et al.*, 1994). The second-order statistics of the considered binary field are thus governed by an exponential autocorrelation function.

Figure 1 shows the binary porosity distribution employed in the numerical analysis. Black regions (material 1) have a porosity, $\phi = 0.05$, and a permeability, $\kappa = 2.69 \times 10^{-3}$ D, while the white regions (material 2) have a porosity, $\phi = 0.4$, and permeability, $\kappa = 3.458$ D. The elastic properties of the dry frame obtained by Eqs. (36) and (37) are shown in Table I.

B. Generic effects of permeability fluctuations

In order to obtain the equivalent flow permeability, we solve the corresponding differential problem [Eqs. (29) to (32)] assuming an externally imposed pressure difference $\Delta p = 100$ Pa. Figure 2 shows the fluid pressure and the normalized modulus of the fluid velocity field for the random medium realization shown in Fig. 1. Note that the fluid pressure field is relatively smooth and is mainly governed by the pressure gradient between the upper and lower boundaries.
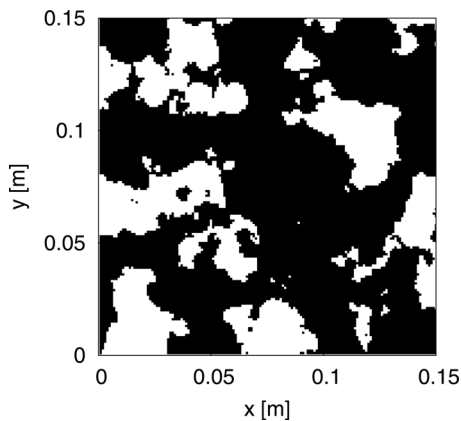

FIG. 1. Heterogeneous binary porosity field considered to analyze the discrepancies between the equivalent seismic permeability and the flow permeability. Black and white regions correspond to porosities of $\phi = 0.05$ and $\phi = 0.4$, respectively.
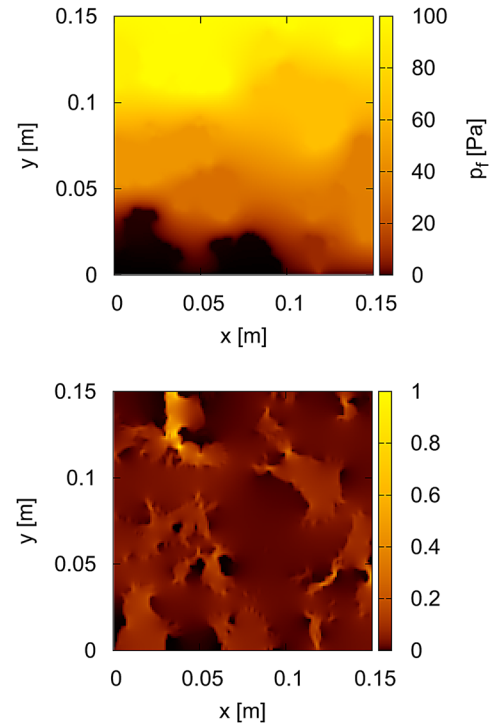

FIG. 2. (Color online) Fluid pressure field (top panel) and normalized modulus of the fluid velocity field (bottom panel) for the numerical rock sample shown in Fig. 1.

Conversely, the fluid velocity field is highly heterogeneous and exhibits fluctuations of three orders-of-magnitude over short distances. It is also interesting to notice that the fluid velocity field is strongly correlated with the pattern shown in Fig. 1. The equivalent flow permeability value given by Eq. (34) turned out to be 7.648×10^{-3} D, which lies between the harmonic (3.903×10^{-3} D) and the arithmetic (1.0738 D) averages.

Figure 3 shows the inverse quality factor and phase velocity curves obtained using the oscillatory compressibility test (solid lines). In order to study the behavior of the seismic permeability, we also include the seismic responses obtained when replacing the heterogeneous permeability field by a homogeneous field having a permeability value given by the arithmetic average (dotted lines), the harmonic average (dotted-dashed lines), and the estimated equivalent flow permeability (dashed lines). Note that while in these cases we consider a homogeneous permeability field, we retain the original heterogeneities associated with the other poroelastic properties, that is, porosity, bulk density, and elastic moduli of the dry frame. We observe that in the presence of permeability fluctuations the attenuation levels are less significant and the attenuation peak gets broader. This is in agreement with the results of Müller *et al.* (2007). In this context, it is interesting and important to note that the same behavior was observed by Yamamoto and Turgut (1988) for classical *P*-wave attenuation in the presence of log-normal pore size distributions. It should, however, also be noted that the effects studied by Yamamoto and Turgut (1988) are produced by pore-scale heterogeneities, while those analyzed in this work arise due to the presence of mesoscale heterogeneities.
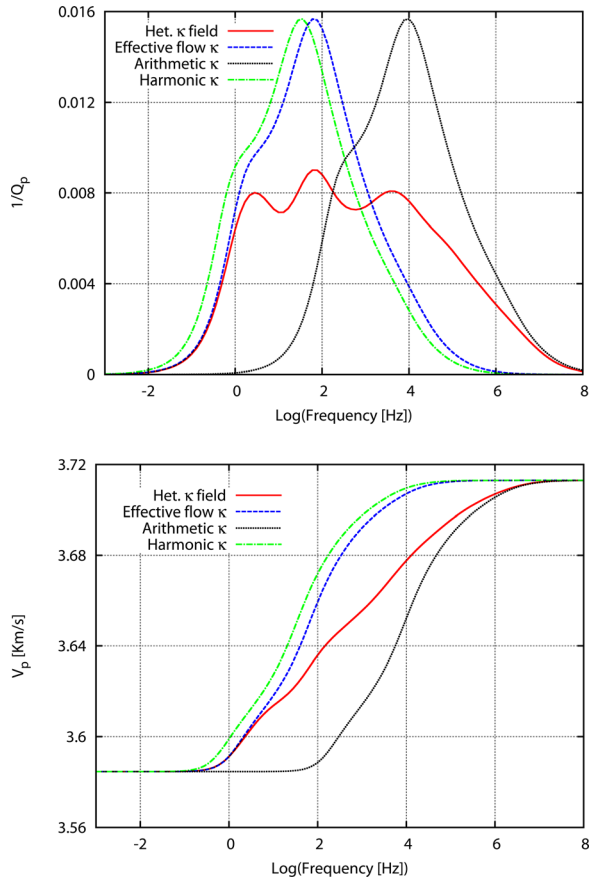
FIG. 3. (Color online) Inverse quality factor (top) and phase velocity (bottom) as functions of frequency for the binary porosity distribution shown in Fig. 1. The different curves correspond to different permeability fields.

We also observe in Fig. 3 that, for frequencies below ~ 1 Hz in the case of the inverse quality factor and below ~ 10 Hz in the case of phase velocity, there is a very good agreement between the responses obtained for the heterogeneous permeability field (solid lines) and those corresponding to a constant permeability value given by the equivalent flow permeability (dashed lines). This, in turn, indicates that for very low frequencies the equivalent seismic permeability is similar to the equivalent flow permeability. This result is expected, since, as explained by Müller *et al.* (2007), at low frequencies the diffusion length is larger than the typical size of the heterogeneities and, hence, WIFF takes place at spatial scales involving several heterogeneities. Conversely, for very high frequencies the diffusion length is much smaller than the typical heterogeneity size and WIFF takes place at spatial scales much smaller than the prevailing heterogeneities. This implies that the local permeability value is sampled which, on average, should yield a seismic permeability close to the arithmetic average. In fact, we observe in Fig. 3 that there is good agreement between the seismic attenuation and phase velocity curves for the heterogeneous permeability field (solid lines) and those corresponding to the arithmetic average of the permeability field (dotted lines), especially for frequencies above $\sim 10^7$ Hz in the case of the inverse quality factor and for frequencies above $\sim 10^6$ Hz in the case of phase velocity. With regard to the

harmonic average permeability, we observe that the attenuation curve is similar to that corresponding to the equivalent flow permeability, although it is shifted toward lower frequencies. For this reason, the harmonic average permeability cannot reproduce the attenuation behavior of the heterogeneous permeability case.

It is interesting to observe that there are three clear attenuation peaks for the heterogeneous permeability field (Fig. 3). Conversely, the averaged permeability fields show two peaks, one of which is very prominent and associated with very high levels of attenuation, while the second one is less visible and related to lower levels of attenuation. In the case of the effective flow permeability, for example, the main attenuation peak is located at a frequency of 63 Hz, while the less prominent one occurs at 3.1 Hz. For this particular averaged permeability, these two attenuation peaks occur at the same frequencies as two of the peaks for the heterogeneous permeability case. In addition, the third attenuation peak for the heterogeneous permeability field is located at approximately the same frequency as the main peak for the arithmetic average permeability. As illustrated by Eq. (2), the occurrence of an attenuation peak due to the presence of mesoscopic heterogeneities manifests the coincidence between the diffusion length and the characteristic size of the heterogeneities (e.g., Gurevich and Lopatnikov, 1995; Müller and Gurevich, 2005a). The fact that the averaged permeability fields exhibit two attenuation peaks, thus points to the existence of two characteristic length scales. However, in the presence of mesoscopic permeability fluctuations, WIFF attenuation is sensitive to the entire permeability range covered by the equivalent seismic permeability. This creates additional possibilities to satisfy Eq. (2), which in turn results in additional attenuation peaks.

The velocity dispersion and attenuation characteristics presented in Fig. 3 are based on a single realization from the corresponding stochastic ensemble. However, we note that in the given context it is possible to obtain meaningful results even from a single realization of the random medium. The reason for this is that WIFF is a local phenomenon occurring in the vicinity of the heterogeneities. The numerical upscaling procedure then averages these local WIFF contributions over the entire sample. So, to some extent, the ensemble averaging process is replaced by the spatial averaging in a single realization. This self-averaging requires that the sample size is large enough so that this single realization is representative of the corresponding stochastic ensemble. The smoothness of the attenuation and velocity dispersion behaviors in Fig. 3 as well as the existence of characteristic frequencies clearly indicate that the sample size is indeed large enough to represent features of the underlying stochastic ensemble.

C. Effects of correlation between permeability field and elastic properties distributions

While it is reasonable to assume that there exists some correlation between the petrophysical material properties, this correlation is unlikely to be as strong as we implicitly assumed in the previous models. Notably, the correlation
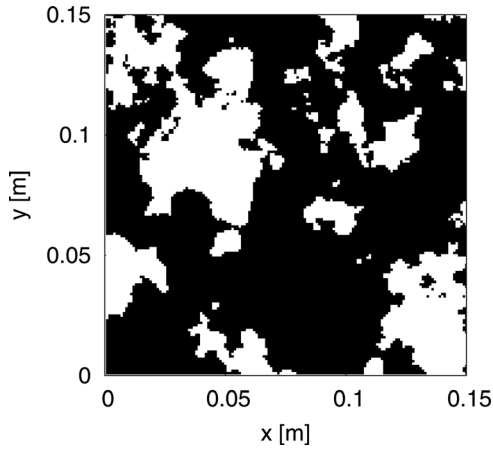
FIG. 4. "Uncorrelated" permeability field used to study the corresponding effects on the attenuation behavior related to the heterogeneous sample shown in Fig. 1. Black and white regions correspond to permeabilities of $\kappa = 2.69 \times 10^{-3}$ D and $\kappa = 3.458$ D, respectively.

between the permeability and the porosity is often found to be rather weak (e.g., Dafflon *et al.*, 2010). To explore the potential implications of such a lack of correlation, we repeat the simulation but consider a different permeability distribution (Fig. 4). That is, we use the permeability field shown in Fig. 4, while keeping the original distributions of all other poroelastic properties, as depicted in Fig. 1.
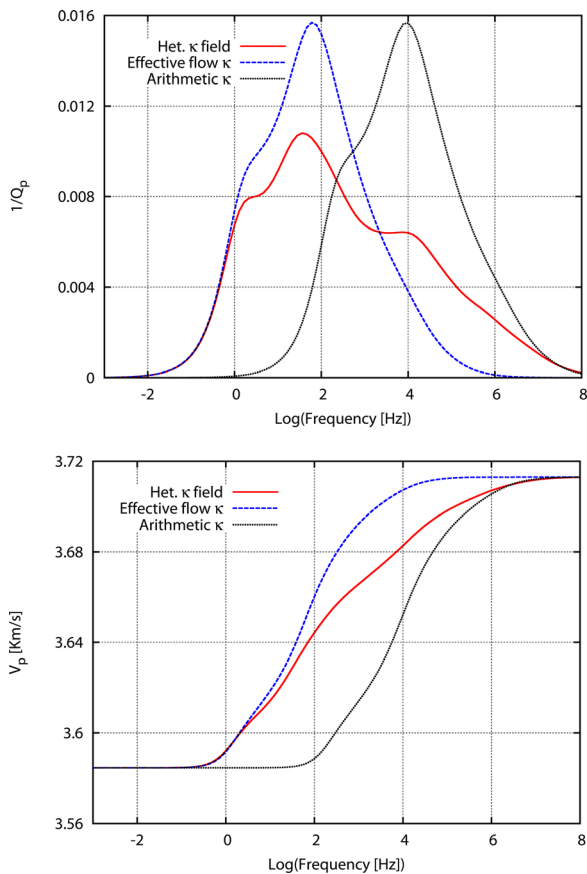

FIG. 5. (Color online) Inverse quality factor (top) and phase velocity (bottom) as functions of frequency for the binary porosity distribution shown in Fig. 1 and the uncorrelated permeability field shown in Fig. 4. The different curves correspond to different permeability fields.

Figure 5 shows the corresponding inverse quality factor and phase velocity as functions of frequency for the equivalent flow permeability (dashed lines), the arithmetic average of the permeability distribution (dotted lines), as well as for the actual heterogeneous permeability field (solid lines). We observe similar results as those shown in the previous simulation. That is, in the presence of strong permeability fluctuations the attenuation levels are less significant and the attenuation peak gets broader. In addition, for very low frequencies the equivalent seismic permeability is similar to the equivalent flow permeability, while for very high frequencies the seismic permeability approaches the arithmetic average value of the sample. These results suggest that our conclusions can indeed be generalized to the case of permeability fields which are uncorrelated with distributions of the porosity and the elastic properties.

D. Effects related to the strength of permeability fluctuations

To analyze the role of the strength of the permeability fluctuations for the equivalent seismic permeability and the corresponding seismic signature, we repeat the first
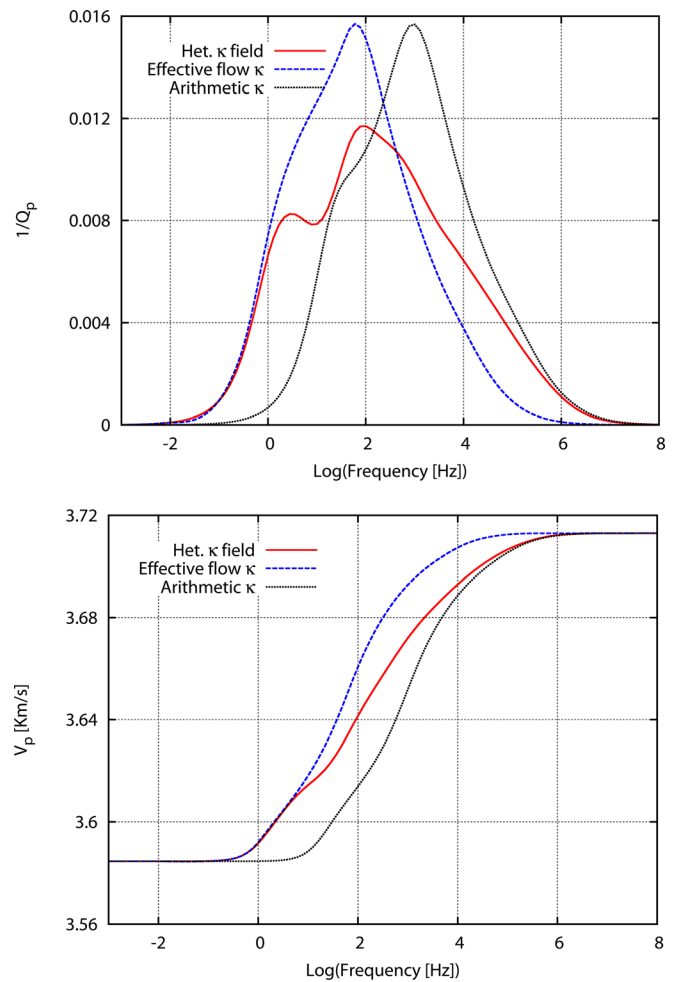

FIG. 6. (Color online) Inverse quality factor (top) and phase velocity (bottom) as functions of frequency for the binary porosity distribution shown in Fig. 1, considering $\kappa = 2.69 \times 10^{-2}$ D for the black regions and $\kappa = 0.3458$ D for the white regions. The different curves correspond to different permeability fields.

simulation with a reduced permeability contrast. This means that for regions having low porosity (black), permeability is $\kappa = 2.69 \times 10^{-2}$ D, that is, ten times the value used in the original simulation. The high-porosity regions (white) correspond to $\kappa = 0.3458$ D, that is, one tenth of the previous value.

Figure 6 shows the inverse quality factor and phase velocity for the heterogeneous permeability field (solid lines), as well as for the arithmetic average of the permeability distribution (dotted lines) and the computed equivalent flow permeability (dashed lines). We observe that for very low frequencies, the equivalent seismic permeability seems to be similar to the equivalent flow permeability, while for very high frequencies it approaches the arithmetic average permeability. Comparing Figs. 3 and 6, we also see that the maximum attenuation is lower for stronger permeability fluctuations. However, the frequency range where attenuation is significant tends to be broader in the strong permeability fluctuations case. Correspondingly, we also observe that significant velocity dispersion effects take place within a broader frequency range for stronger permeability fluctuations.

IV. CONCLUSIONS

We have explored the effects of strong permeability fluctuations on the P-wave attenuation and velocity dispersion of heterogeneous porous rocks. To this end, we numerically determined compressional wave attenuation and velocity dispersion due to WIFF in 2D random poroelastic medium realizations with realistic spatial fluctuations of the poroelastic properties, including strong permeability contrasts. Particular attention was given to the role of the equivalent seismic permeability that reproduces the acoustic response of the original heterogeneous porous medium if the permeability field is replaced by an upscaled, constant permeability. In order to infer the behavior of the equivalent seismic permeability, we compared the acoustic responses of heterogeneous porous media with those obtained by replacing the heterogeneous permeability fields by constant values, including the corresponding arithmetic and harmonic averages, as well as the equivalent flow permeability. The latter was obtained by numerically solving the steady-state flow equation for the same 2D random medium realizations. The numerical examples shown in this work can be regarded as representative for the considered stochastic models and, hence, allow for the following conclusions:

(i) Strong permeability fluctuations, characterized by ratios on the order of 10^3 between the maximum and minimum values, diminish the magnitude of WIFF attenuation compared to poroelastic media with constant permeability, but otherwise heterogeneous parameters. These lower levels of attenuation are accompanied with a broadening of the attenuation peak as well as a broadened velocity dispersion behavior. These effects are more significant as the strength of the permeability fluctuations increases. This also means that the observability of attenuation

and dispersion within a certain frequency band is controlled by permeability fluctuations.

(ii) At very low frequencies ($\omega \ll \omega_c$), the equivalent seismic permeability is similar to the equivalent flow permeability. At very high frequencies ($\omega \gg \omega_c$), the equivalent seismic permeability approaches the arithmetic average of the permeability field. This also confirms that the equivalent seismic permeability is frequency-dependent and, hence, warrants the concept of dynamic-equivalent permeability in poroelastic media with mesoscale heterogeneities.

(iii) The results described under points (i) and (ii) above also hold true for random permeability fields which are not correlated with the spatial fluctuations of the porosity and the associated poroelastic material properties.

Our findings have implications concerning the possibility of estimating the equivalent flow permeability of geological formations using seismic waves. Seismic signatures are controlled by an equivalent seismic permeability, which can be very different from the equivalent flow permeability. This difference is controlled by the strength of the mesoscopic permeability fluctuations. Given that in many geological formations the permeability fluctuations are strong, often exhibiting orders-of-magnitude between the minimum and maximum values, it is important to understand the scaling relation between these two equivalent permeabilities. This study shed some light onto the controlling factors for the equivalent seismic permeability. Future work will focus on the scaling relation to enable predictions of the equivalent flow permeability from seismic signatures.

Berryman, J. G. (**1986**). "Elastic wave attenuation in rocks containing fluids," Appl. Phys. Lett. **49**, 552–554.

Berryman, J. G. (**1988**). "Seismic wave attenuation in fluid-saturated porous media," Pure Appl. Geophys. **128**, 423–432.

Biot, M. A. (**1941**). "General theory of three-dimensional consolidation," J. Appl. Phys. **12**, 155–164.

Biot, M. A. (**1956a**). "Theory of propagation of elastic waves in a fluid saturated porous solid. I. Low frequency range," J. Acoust. Soc. Am. **28**, 168–178.

Biot, M. A. (**1956b**). "Theory of propagation of elastic waves in a fluid saturated porous solid. II. Higher frequency range," J. Acoust. Soc. Am. **28**, 179–191.

Caspari, E., Müller, T. M., Rubino, J. G., and Gurevich, B. (**2013**). "Biot's slow wave and effective hydraulic conductivity in random media," Poromechanics **V**, 217–226.

Chandler, R. N., and Johnson, D. L. (**1981**). "The equivalence of quasistatic flow in fluid-saturated porous media and Biot's slow wave in the limit of zero frequency," J. Appl. Phys. **52**, 3391–3395.

Dafflon, B., Irving, J., and Holliger, K. (**2010**). "Calibration of high-resolution geophysical data with tracer test measurements to improve hydrological predictions," Adv. Water Resour. **33**, 55–68.

Desbarats, A. J. (**1992**). "Spatial averaging of hydraulic conductivity in three-dimensional heterogeneous porous media," Math. Geol. **24**, 249–267.

Dutta, N. C., and Odé, H. (**1979**). "Attenuation and dispersion of compressional waves in fluid-filled porous rocks with partial gas saturation (White model)—Part I: Biot theory," Geophysics **44**, 1777–1788.

Goff, J. A., Holliger, K., and Levander, A. (**1994**). "Modal fields: A new method for characterization of random seismic velocity heterogeneity," Geophys. Res. Lett. **21**, 493–496, doi:10.1029/94GL00311.

Guarracino, L., and Monachesi, L. B. (**2010**). "Numerical simulation of constitutive relations for unsaturated flow in fractured porous media," in *Proceedings of XVIII Conference on Computational Methods in Water Resources (CMWR 2010)*, pp. 1–8.

Gurevich, B., and Lopatnikov, S. L. (**1995**). "Velocity and attenuation of elastic waves in finely layered porous rocks," Geophys. J. Int. **121**, 933–947.

Holliger, K., Levander, A., and Goff, J. A. (**1993**). "Stochastic modeling of the reflective lower crust: Petrophysical and geological evidence from the Ivera zone (Northern Italy)," J. Geophys. Res. **98**, 11967–11980, doi:10.1029/93JB00351.

Johnson, D. L., Koplik, J., and Dashen, R. (**1987**). "Theory of dynamic permeability and tortuosity in fluid-saturated porous media," J. Fluid Mech. **176**, 379–402.

Krief, M., Garat, J., Stellingwerff, J., and Ventre, J. (**1990**). "A petrophysical interpretation using the velocities of P and S waves (full waveform inversion)," Log Analyst **31**, 355–369.

Mavko, G., Mukerji, T., and Dvorkin, J. (**2009**). *The Rock Physics Handbook: Tools for Seismic Analysis of Porous Media*, 2nd ed. (Cambridge University Press, New York), pp. 1–524.

Müller, T. M., and Gurevich, B. (**2005a**). "Wave-induced fluid flow in random porous media: Attenuation and dispersion of elastic waves," J. Acoust. Soc. Am. **117**, 2732–2741.

Müller, T. M., and Gurevich, B. (**2005b**). "A first-order statistical smoothing approximation for the coherent wave field in random porous media," J. Acoust. Soc. Am. **117**, 1796–1805.

Müller, T. M., Gurevich, B., and Lebedev, M. (**2010**). "Seismic wave attenuation and dispersion resulting from wave-induced flow in porous rocks—A review," Geophysics **75**, 75A147–75A164.

Müller, T. M., Lambert, G., and Gurevich, B. (**2007**). "Dynamic permeability of porous rocks and its seismic signatures," Geophysics **72**, E149–E158.

Müller, T. M., and Sahay, P. N. (**2011**). "Stochastic theory of dynamic permeability in poroelastic media," Phys. Rev. E **84**, 026329.

Pride, S. R., Berryman, J. G., and Harris, J. M. (**2004**). "Seismic attenuation due to wave-induced flow," J. Geophys. Res. **109**, B01201, doi:10.1029/2003JB002639.

Quintal, B., Steeb, H., Frehner, M., and Schmalholz, S. M. (**2011**). "Quasi-static finite element modeling of seismic attenuation and dispersion due to wave-induced fluid flow in poroelastic media," J. Geophys. Res. **116**, B01201, doi:10.1029/2010JB007475.

Rubino, J. G., Ravazzoli, C. L., and Santos, J. E. (**2009**). "Equivalent viscoelastic solids for heterogeneous fluid-saturated porous rocks," Geophysics **74**, N1–N13.

Rubino, J. G., Santos, J. E., Picotti, S., and Carcione, J. M. (**2007**). "Simulation of upscaling effects due to wave-induced fluid flow in Biot media using the finite-element method," J. Appl. Geophys. **62**, 193–203.

Rubino, J. G., Velis, D. R., and Holliger, K. (**2012**). "Permeability effects on the seismic response of gas reservoirs," Geophys. J. Int. **189**, 448–468.

Sanchez-Vila, X., Guadagnini, A., and Carrera, J. (**2006**). "Representative hydraulic conductivities in saturated groundwater flow," Rev. Geophys. **44**, RG3002, doi:10.1029/2005RG000169.

Shapiro, S. A., and Müller, T. M. (**1999**). "Seismic signatures of permeability in heterogeneous porous media," Geophysics **64**, 99–103.

Tronicke, J., and Holliger, K. (**2005**). "Quantitative integration of hydrogeophysical data: Conditional geostatistical simulation for characterizing heterogeneous alluvial aquifers," Geophysics **70**, H1–H10.

van Dalen, K. N., Ghose, R., Drijkoningen, G. G., and Smeulders, D. M. J. (**2010**). "In-situ permeability from integrated poroelastic reflection coefficients," Geophys. Res. Lett. **37**, L12303, doi:10.1029/2010GL043319.

Wang, H. F. (**2000**). *Theory of Linear Poroelasticity with Applications to Geomechanics and Hydrogeology* (Princeton University Press, Princeton), pp. 1–287.

Wenzlau, F., Altmann, J. B., and Müller, T. M. (**2010**). "Ansiotropic dispersion and attenuation due to wave-induced flow: Quasi-static finite-element modeling in poroelastic solids," J. Geophys. Res. **115**, B07204, doi:10.1029/2009JB006644.

Yamamoto, T., and Turgut, A. (**1988**). "Acoustic wave propagation through porous media with arbitrary pore size distributions," J. Acoust. Soc. Am. **83**, 1744–1751.